Enhancement of superconductivity on thin film of Sn under high pressure

Misaki Sasaki[1], Masahiro Ohkuma[2],* Ryo Matsumoto[2], Toru Shinmei[3], Tetsuo Irifune[3], Yoshihiko Takano[2], and Katsuya Shimizu[1]
[1]*KYOKUGEN, Graduate School of Engineering Science, Osaka University, Toyonaka, Osaka, 560-8531, Japan*
[2]*Research Center for Materials Nanoarchitectonics (MANA), National Institute for Materials Science, Tsukuba 305-0047, Ibaraki, Japan and*
[3]*Geodynamics Research Center, Ehime University, Matsuyama, 790-8577, Ehime, Japan*
(Dated: January 30, 2025)

We investigated the pressure effects of a superconductivity on thin films of Sn. Elemental superconductor Sn with a body-centered tetragonal structure, β-Sn, exhibits superconductivity below the superconducting transition temperature (T_c = 3.72 K) at ambient pressure. T_c of Sn increases with lowering dimension such as in thin film and nanowire growth, or by high-pressure application. For thin films, T_c exhibits a slight increase up to approximately 4 K compared to the bulk value, attributable to the crystalline size and lattice disorder. By applying pressure on a bulk Sn, T_c decreases with increasing pressure from 3.72 K to 5.3 K with the structural transformation into γ-Sn around 10 GPa. However, the combination of these effects on thin films of Sn, namely, thin-film growth and pressure effects, remains underexplored. In this study, we combined film-growth and pressure-application techniques to further increase T_c using a diamond anvil cell with boron-doped diamond electrodes. The drop of the electrical resistance suggesting the onset of T_c on the thin film reached above 6 K in γ-Sn phase. Further, the upper critical magnetic field was drastically enhanced. Atomic force microscopy suggests that the refinement of the grain size of the thin film under the non-hydrostatic pressure conditions contributes to stabilizing the higher T_c of γ-Sn.

I. INTRODUCTION

Applying high pressures to directly compress a material is a useful approach to investigate intriguing physical properties and search for new materials [1, 2]. For instance, oxygen—a gas at ambient conditions— exhibits metallic behaviors and superconductivity at high pressures [3, 4]. Recently, high-temperature superconductors such as hydrogen-rich materials and nickelates under high pressure have attracted considerable attention [5–18]. In addition, recent discoveries of the high-temperature superconducting states in elemental solid Ti and Sc at extreme pressures imply the potential of high-temperature superconductivity in high-pressure phases of other elements [19–21].

Some elemental superconductors with thin-film dimensions show an increase in superconducting transition temperature (T_c) compared to the bulk value, attributable to the crystalline size and lattice disorder [22–25]. In the case of Sn, T_c for thin films and nano-wires varies slightly depending on the size and surface morphology [26–29]. The mechanism of T_c enhancement is not thoroughly clear although it has been proposed to arise from changes in the phonon density of states, the electron density of states, and the electron-phonon coupling [30–32].

Sn exhibits various crystal structures at high pressures [33–35]. Half a century ago, Wittig investigated the electrical transport properties of bulk Sn at high pressures of up to 16 GPa and revealed the highest T_c is 5.3 K at 11.3 GPa on the pressure induced phase, γ-Sn, where β-Sn shows superconductivity below 3.72 K at ambient pressure [36]. However, research on combination of pressure application and thin-film growth on elemental superconductors is inadequate. Here, we hypothesize that changing the crystalline size of a thin film via pressure application could stabilize the higher T_c.

In this study, we combined thin film growth and pressure-application techniques to increase T_c using a diamond anvil cell (DAC) with boron-doped diamond (BDD) electrodes [37–39]. We investigated the pressure effects on superconductivity of thin films of Sn compared to the bulk sample. We observed a higher T_c for the thin film comapred to previous studies on high-pressure phase. Further, we observed a drastically enhanced critical magnetic field on the thin film under high pressure.

II. EXPERIMENTAL PROCEDURE

Thin films of Sn were deposited on a diamond anvil by a resistance heating evaporation. The target metal was a high-purity Sn, purchased from Kojundo Chemical Lab. Co. Ltd. Comparing with the high pressure measurements, we also prepared Sn thin film on a diamond substrate for electrical transport measurements at ambient pressure. The film deposition on two diamonds was performed simultaneously. The optical images of the thin films on the diamond anvil and the diamond substrate are shown in Fig. 1(a) and the inset of Fig. 1(c), respectively. The film thickness and surface morphology of the films were evaluated via atomic force microscopy (AFM; Nanocute, SII NanoTechnology Inc.) at room tempera-

* Present address: School of Engineering, Institute of Science Tokyo, Yokohama, Kanagawa 226-8501, Japan

ture. For the magnetic measurements of the bulk Sn, a wire of high-purity Sn (Nilaco Corp.) was used.

High-pressure generation was performed using DAC. The pressure value at room temperature was evaluated using ruby fluorescence and Raman shift of diamond [40, 41]. In the electrical transport measurements, diamond anvil with BDD electrodes with a culet size of 300 μm was used [37–39]. The BDD electrodes were deposited homoepitaxially on the diamond anvil by microwave plasma chemical vapor deposition [42]. This electrode exhibits high durability and can be reused until the diamond anvil itself fractures. Further, thin films could be deposited directly on the diamond anvil with BDD electrodes, eliminating the need for an electrode fabrication process after thin film deposition [37, 43, 44]. The pressure-transmitting media in the solid, liquid, and gaseous states are compatible with this system. A gasket of a stainless steel was pre-indented and a 200 μm diameter hole was drilled. The insulating layer was prepared using a MgO–epoxy mixture. We termed this setup as non-hydrostatic. We also performed the high-pressure generation with better hydrostatic pressure condition than non-hydrostatic measurement using a liquid pressure-transmitting medium, glycerol. A 150 μm diameter hole was drilled in the insulating layer of MgO–epoxy mixture to prepare the sample space, which was filled with glycerol. We termed this setup as quasi-hydrostatic. In quasi-hydrostatic pressure measurements, the pressure value was evaluated using Raman shift of diamond [41]. The electrical transports under a magnetic field (H) perpendicular to the surface were measured by a four-terminal method by physical properties measurement system (Quantum Design).

For magnetic measurements, we used a miniature DAC in combination with a superconducting quantum interference device magnetometer (MPMS, Quantum Design) [45–50]. A nano-polycrystalline diamond with culet size of 600 μm and a pre-indented tungsten gasket with a hole size of 200 μm were used [51]. Bulk Sn pieces and ruby powders were loaded into the sample space without a pressure-transmitting medium. The in-phase component of the AC magnetic response (m') was measured. The frequency and amplitude of the AC field were 3 Hz and 0.2 mT, respectively.

III. EXPERIMENTAL RESULTS

A. Ambient pressure

Figure 1(b) shows the temperature (T) dependence of m' for the bulk Sn under H, where no background signal from DAC is subtracted. Below 3.7 K, the diamagnetic signal suggesting the superconducting state was observed at $H = 0$. The T_c onset was decreased by applying H. Figure 1(c) shows the T dependence of the electrical resistance (R) under H perpendicular to the film surface. The residual resistance ratio (RRR) was estimated to be 11. At $H = 0$, an R drop suggesting the onset of the superconducting transition was observed at 3.75 K. T_c slightly increased compared to the bulk value and was similar to values from the previous studies on thin films [27, 28]. By applying H, the onset of T_c decreased with increasing H. However, the critical magnetic field was three times higher than that of the bulk Sn (Fig. 1(d)). H_c of 100 mT estimated using $H_c(T) = H_c(1 - (T/T_c)^2)$ was similar to that of a previous study [28]. Considering to the H_c, the thin film transformed into a type II superconductor, as previously reported [28, 52, 53].

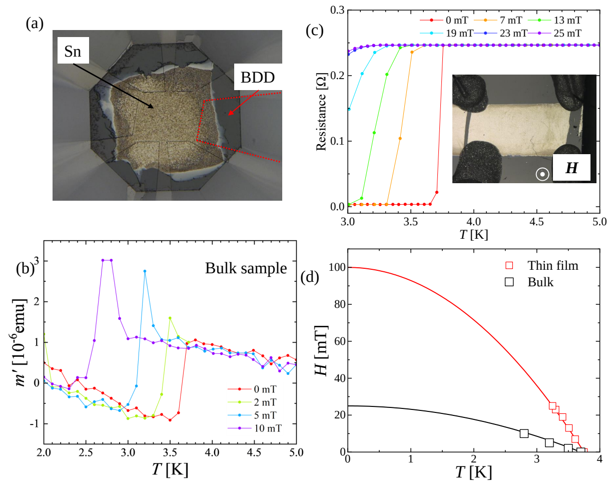

FIG. 1. (Color online) (a) Optical image of the thin film of Sn on the diamond anvil with BDD electrodes. The dotted area indicates one of the BDD electrodes. (b) T dependence of the in-phase component of m' on the bulk Sn. (c) T dependence of R on the thin film of Sn on the diamond substrate. The magnetic field was applied perpendicularly to film. The inset shows the optical image of the thin film of Sn on the diamond substrate (d) T dependence of the critical magnetic field on thin film and bulk Sn.

B. Non-hydrostatic pressure on bulk Sn

Figure 2(a) shows the T dependence of m' on the bulk Sn under high pressures. On applying pressure, T_c decreased, as previously reported. Figure 2(b) shows the T dependence of m' at 2.7 GPa under varying H. The decrease of T_c was observed by applying $H = 2$ mT. At $H = 10$ mT, T_c was below 2 K. H_c was evaluated to be 13 mT, as shown in the inset of Fig. 2(b).

C. Non-hydrostatic pressure on thin film

Figure 3(a) shows the T dependence of R on the thin film of Sn under high pressures on pressurization. As shown in the inset of Fig. 4(a), RRR was estimated to be 1.4 at 2.5 GPa, which was much lower than that under ambient pressure. We speculate that the crystallographic

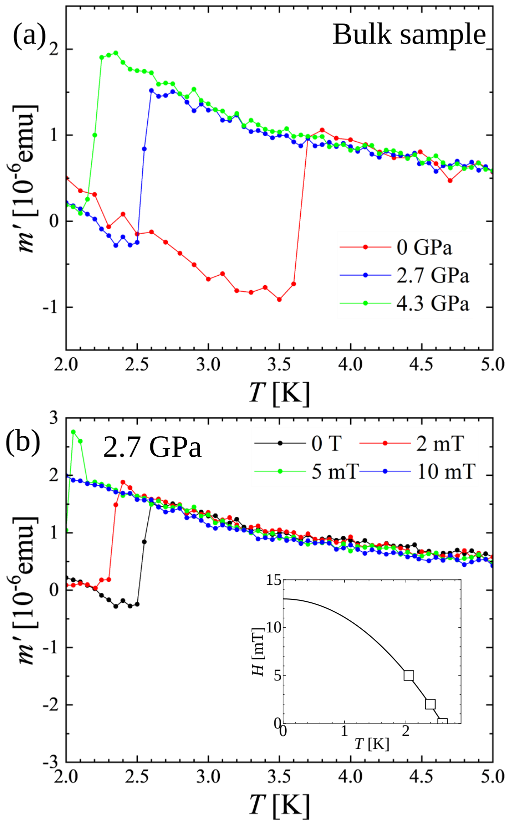

FIG. 2. (Color online) (a) T dependence of m' on bulk Sn under high pressures. (b) T dependence of m' at 2.7 GPa under varying magnetic fields. The inset shows the T dependence of the critical magnetic field.

defect was introduced because of the non-hydrostatic pressure condition. The R drop suggesting the superconducting transition was observed around 4 K, whereas T_c was 3.75 K under ambient pressure. T_c decreased on further increasing the pressure, as previously reported. R showed peak behavior just above T_c at 5.5 GPa, possibly due to the granularity or disorder on the thin films. Above 9.5 GPa, R slightly tended to decrease around 6 K, suggesting the superconducting transition, where γ-Sn phase could emerge. With further pressure application, the R drop became significant, and T_c slightly decreased. After applying 20 GPa, the pressure was decreased to 10.5 GPa. Figure 3(b) shows the T dependence of R for the thin film of Sn under high pressures with depressurization. The onset of T_c increased to 6.3 K at 10.5 GPa, and γ-Sn remained at 8.5 GPa. γ-Sn vanished when the pressure was decreased to 3.5 GPa.

Figures 4(a) and (b) show the T dependence of R for the thin film of Sn under various H at 2.5 and 10.5 GPa under non-hydrostatic pressure condition. T_c was observed at 1 T, whereas the upper critical magnetic field (H_{c2}) was approximately 0.1 T under ambient pressure. Drastic H_{c2} enhancement was also observed in the γ phase at 10.5 GPa. As shown in Fig. 4(c), H_{c2} estimated using Werthamer–Helfand–Hohenberg (WHH) model reached several teslas at high pressures [54–56]. Notably, the H_{c2} enhancement of β-Sn under the non-hydrostatic pressure condition was observed reproducibly. Figure 5(b) shows the T dependence of R for the thin film of Sn with the other setup at 5 GPa. The optical image of the thin film of Sn is shown in Fig. 5(a). The R decrease suggesting the superconducting transition was observed even at $H = 1.0$ T. The enhancement of H_{c2} is thought to originate from the shortening in the mean free path of the electrons and the resulting shortening in the coherence length. The RRR was estimated to be 11 under ambient pressure; however, it decreased to 1.4 under non-hydrostatic pressure condition, indicating that the mean free path of the electrons shortened.

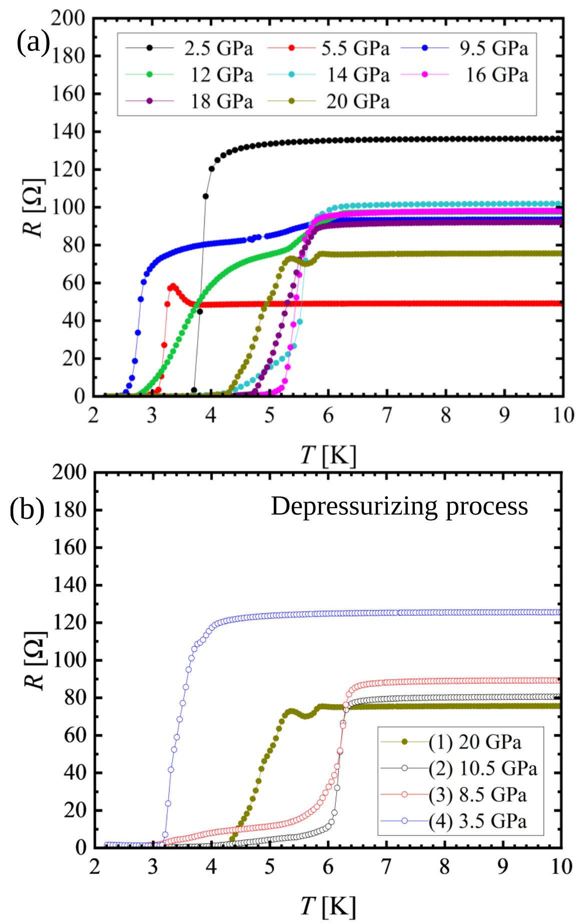

FIG. 3. (Color online) T dependence of electrical R under non-hydrostatic pressure with (a) pressurizing process (b) depressurizing process. The number in (b) indicates the order of measurements.

D. Quasi-hydrostatic pressure on thin film

We performed high-pressure generation with better hydrostatic pressure condition using a liquid pressure trans-

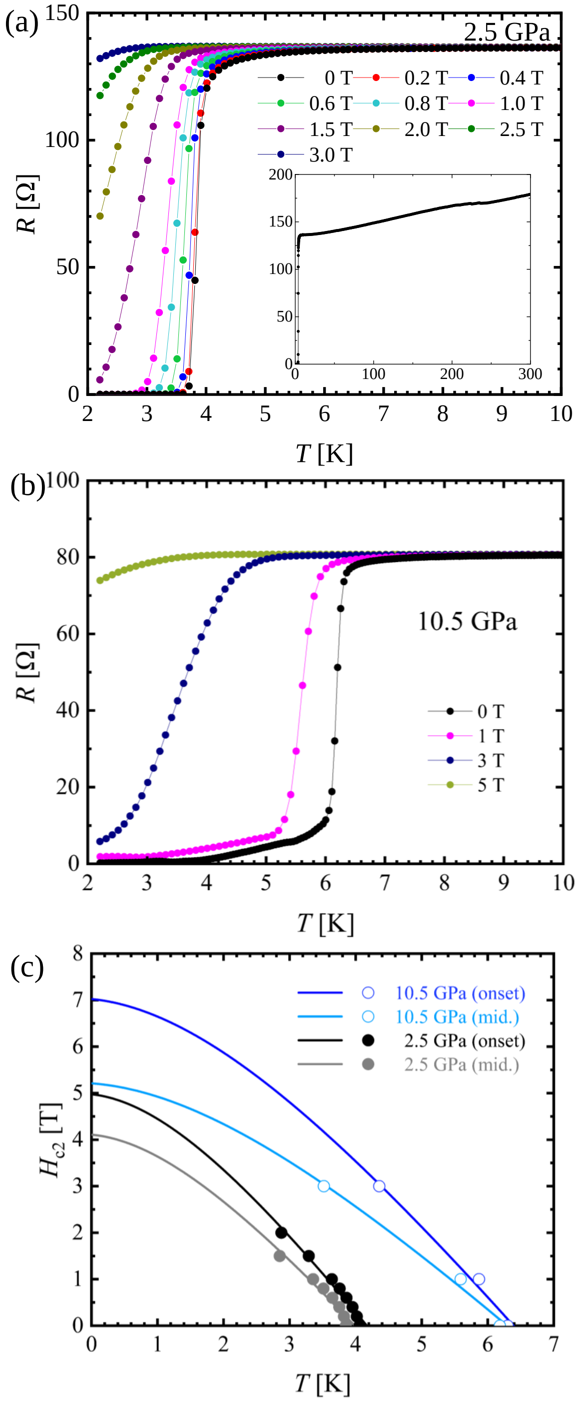

FIG. 4. (Color online) (a) and (b) T dependence of R under the magnetic field at (a) 2.5 and (b) 10.5 GPa. The inset of (a) shows T dependence of R between 2 and 300 K at 2.5 GPa without the external magnetic field. (c) T dependence of the upper critical magnetic field at 2.5 and 10.5 GPa. The solid lines represent the fitting curves estimated by the WHH model.

mitted medium, glycerol. Figure 6(a) shows the R–T of the thin film at 9 GPa under quasi-hydrostatic pressure conditions. The optical image of the thin film in-

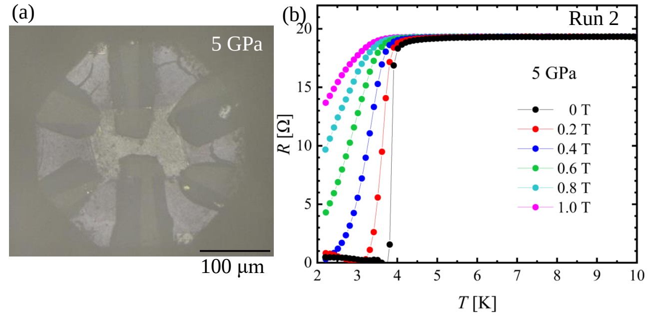

FIG. 5. (Color online) (a) Optical image of the thin film of Sn at 5 GPa and (b) T dependence of R at 5 GPa.

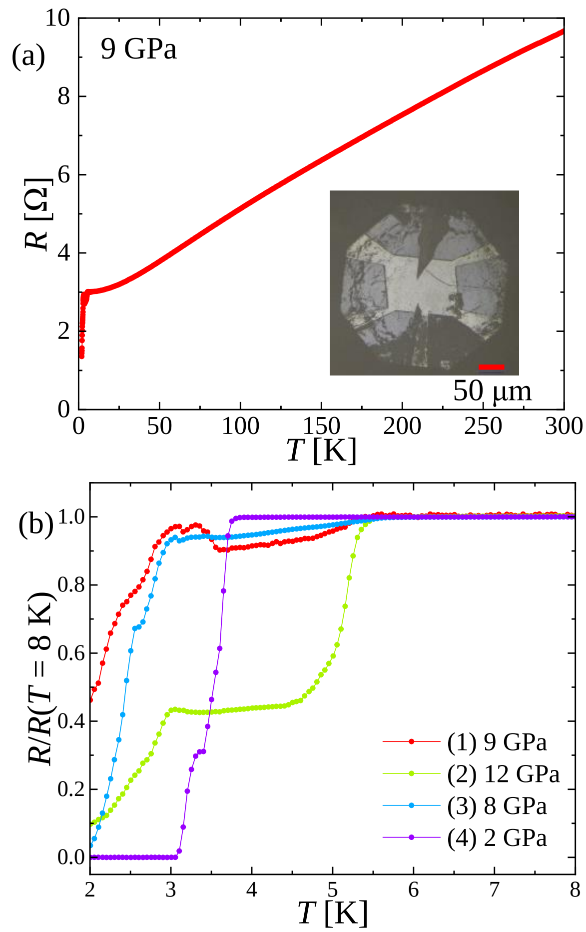

FIG. 6. (Color online) (a) T dependence of R at 9 GPa. The inset shows the optical image of the thin film. (b) T dependence of R under high pressures between 2 and 8 K.

side the DAC is shown in the inset of Fig. 6(a). The RRR was with in 2—3 in quasi-hydrostatic pressure measurements, which was slightly higher than those for the non-hydrostatic pressure condition. The R drop suggesting superconducting transition was observed around 5 K. Figure 6(b) shows R–T under quasi-hydrostatic pressure condition between 2 and 8 K with warming process.

The R value was normalized using the value at 8 K. At 9 GPa, R slightly decreased with decreasing T around 5.3 K, suggesting the superconducting transition on γ-Sn. The R drop was also observed around 3 K. The γ-Sn phase became significant on further pressure application. The onset of T_c slightly increased at 12 GPa. We also decreased the pressure from 12 to 8 GPa. The R decrease suggesting the superconducting transition of γ-Sn was slightly observed, whereas the γ-Sn was clearly observed at 8.5 GPa under the non-hydrostatic pressure condition. With further pressure decrease, γ-Sn vanished at 2 GPa.

IV. DISCUSSION

A. Pressure dependence of T_c

Figure 7 shows the pressure dependence of T_c for the thin film and bulk samples compared with results from a previous study [36]. For the bulk Sn, the behavior of T_c with respect to pressure was good agreement with the previous study. A similar tendency was observed for the thin film in β-Sn phas;, however, its T_c was higher compared to bulk Sn. One possible reason is the geometry of the thin film. As shown in Fig 1(a), the thin film area occupies approximately 70% of the culet of the diamond anvil, which produces the pressure distribution. In the γ-Sn phase, T_c with quasi-hydrostatic pressure measurements showed a trend similar to the previous results [36]. Meanwhile, T_c with non-hydrostatic pressure showed a higher value. We observed the highest T_c of 6.3 K at 10.5 GPa, which was approximately 10% higher than that reported in a previous study [36]. The highest T_c is not fully explained by the pressure gradient. Assuming that the T_c of bulk γ-Sn continues to change at a rate of -0.11 K/GPa, it is necessary to decrease the pressure to 4 GPa from the γ phase above 10 GPa. However, the γ phase cannot exist metastably under this pressure as was observed during the γ to β phase transition on the decompression process (Fig. 3(b)). We emphasize that we observed the mid point of T_c to be greater than 6.0 K (Fig. 4(b)).

B. Atomic force microscopy

To investigate the morphology on the thin films, we performed AFM measurements before and after applying pressure under the non-hydrostatic pressure condition. Figures 8(a) and (b) show the optical and AFM images of the thin film before pressurization. The thin film of Sn was deposited on a diamond anvil without BDD electrodes. The average film thickness was evaluated to be 70 nm. A magnified AFM image is shown in Fig. 8(c). The average grain size was estimated to be approximately 300 nm. Figure 8(d) shows the optical image of the thin film after applying pressure up to 4.2 GPa. The pressure was evaluated by the diamond Raman shift.

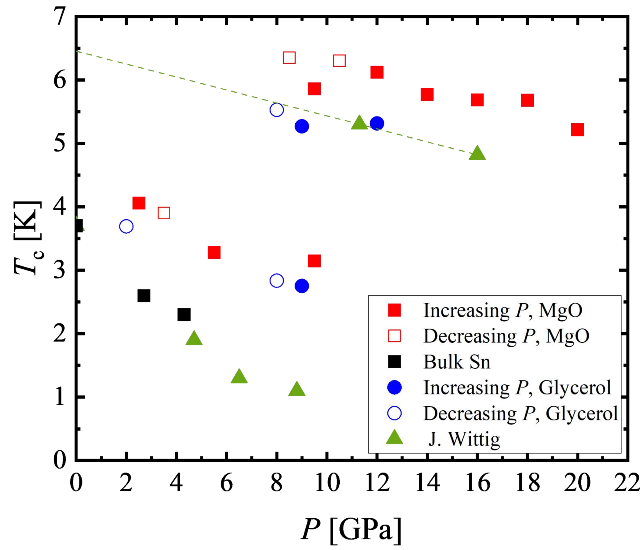

FIG. 7. (Color online) Pressure dependence of the superconducting transition temperature. The green triangles indicate the results by Wittig [36]. The dotted line indicates a guide for the eyes.

Most of the thin film peeled off and was transferred to the MgO–epoxy mixture. We measured the small remaining thin-film area. Figure 8(e) shows the AFM image of the thin film after pressurization. The average film thickness was evaluated to be 60 nm. A magnified view is shown in Fig. 8(f). The grain size was reduced to several tens of nanometers on pressure application.

Next, we performed AFM measurements under quasi-hydrostatic pressure condition for comparison with the non-hydrostatic pressure measurements. The thin film was the same as that used in the R–T measurement. Figures 9(a) and (b) show the AFM images of the thin film before applying pressure. The average thickness and average grain size were evaluated to be 82 and 600 nm, respectively. Figures 9(c) and (d) show the AFM images on the thin film after applying pressure up to 12 GPa. The pressure-transmitting medium was removed using ethanol and nitrogen gas. The average thickness was evaluated to be 91 nm. Unlike the non-hydrostatic pressure measurements, grain refinement was not observed.

The AFM results revealed that the grain refinement was observed only under the non-hydrostatic pressure condition. In the R–T results, the maximum T_c value under the non-hydrostatic condition was 10% higher than that under the quasi-hydrostatic condition, suggesting that the grain refinement plays a pivotal role in stabilizing the higher T_c. Smaller grain sizes tend to have higher T_c, because of phonon softening under ambient pressure [32]. Houben *et al.* performed nuclear resonant inelastic x-ray scattering on nano-structured films and bulk Sn to investigate the phonon density of states and observed a decrease in the high-energy phonon modes and a slight increase in the low-energy phonon modes in nano-structured films [31, 32]. Using the obtained phonon spectra, calculations based on the Allen–Dynes–McMillan formalism yielded T_c values in good agreement with the experimental data. In nano-structured films, the electron–phonon coupling increased by up to 10%, suggesting that phonon softening and the associated change in electron–phonon coupling play a major role in the T_c increase. We consider that the T_c increase under the non-hydrostatic pressure condition is related to the grain size and that grain refinement could induce to changes in electron-phonon coupling.

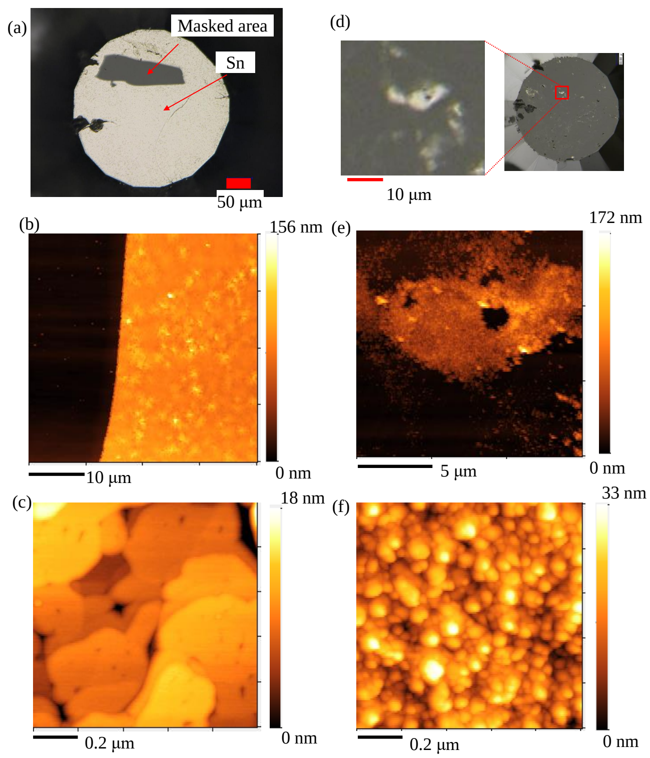

FIG. 8. (Color online) (a) Optical image of the thin film of Sn on a diamond anvil before pressurization. (b) and (c) AFM image on the thin film before pressurization. (d) Optical images of the thin film of Sn on the diamond anvil after pressurization. (e) and (f) AFM image of the thin film after pressurization.

C. Possible higher T_c on Sn

Recently, anomalies in magnetization, resistance, and heat capacity suggesting the superconducting transition were observed around 5.5 K in nano-wires of Sn [57]. Further, based on scanning tunneling microscopy, the thin film of Sn deposited on $SrTiO_3$ substrate exhibited superconductivity around 8 K [58]. Indeed, in our thin film, the decrease of R was observed at 11 K under 9.5 GPa, suggesting the signature of the superconducting transition, and the anomaly shifted to lower T by applying the

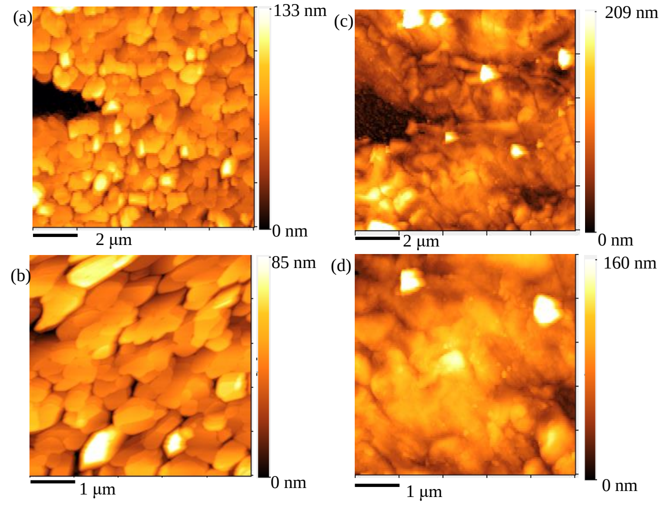

FIG. 9. (Color online) AFM under quasi-hydrostatic pressure condition. (a) and (b) AFM image of the thin film before pressurization. (c) and (d) AFM image of the thin film after pressurization.

magnetic field (Fig 10). On the other hand, some granular or amorphous thin films exhibit a resistance decrease at higher T than T_c due to the effects of fluctuations [59–62]. Further investigations such as magnetic measurements [63, 64], heat capacity measurements [65], and scanning tunneling microscopy [66] under high pressure may offer insights for the possible stabilization of higher T_c.

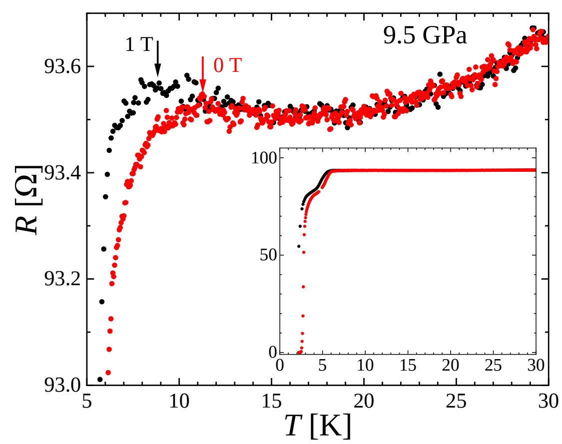

FIG. 10. (Color online) Temperature dependence of the electrical resistance at 9.5 GPa. The downward arrows indicate the onset of the anomalies in the resistance.

V. CONCLUSION

In conclusion, we demonstrated the pressure effect on the superconductivity of thin films of Sn. We observed the superconductivity below 6.3 K in the γ-phase of Sn, which was approximately 10% higher than previous bulk results. Further, the H_{c2} drastically increased under the non-hydrostatic high pressure condition. We also observed the signature of the superconducting transition at higher T than T_c. AFM results suggest that the grain refinement under non-hydrostatic pressure contributes to the stabilization of the higher T_c of γ-Sn.

ACKNOWLEDGMENTS

This work was supported by JSPS KAKENHI Grant No. 19H02177, 20H05644 and JST-Mirai Program Grant No. JPMJMI17A2. This work was also supported by the Joint Usage/Research Center PRIUS, Ehime University, Japan

---

[1] H.-K. Mao, X.-J. Chen, Y. Ding, B. Li, and L. Wang, Rev. Mod. Phys. **90**, 015007 (2018).
[2] S. Yamanaka, Dalton Trans. **39**, 1901 (2010).
[3] K. Shimizu, K. Suhara, M. Ikumo, M. I. Eremets, and K. Amaya, Nature **393**, 767 (1998).
[4] K. Shimizu, K. Amaya, and N. Suzuki, J. Phys. Soc. Jpn. **74**, 1345 (2005).
[5] A. P. Drozdov, M. I. Eremets, I. A. Troyan, V. Ksenofontov, and S. I. Shylin, Nature **525**, 73 (2015).
[6] A. P. Drozdov, P. P. Kong, V. S. Minkov, S. P. Besedin, M. A. Kuzovnikov, S. Mozaffari, L. Balicas, F. F. Balakirev, D. E. Graf, V. B. Prakapenka, E. Greenberg, D. A. Knyazev, M. Tkacz, and M. I. Eremets, Nature **569**, 528 (2019).
[7] M. Somayazulu, M. Ahart, A. K. Mishra, Z. M. Geballe, M. Baldini, Y. Meng, V. V. Struzhkin, and R. J. Hemley, Phys. Rev. Lett. **122**, 027001 (2019).
[8] R. Matsumoto, M. Einaga, S. Adachi, S. Yamamoto, T. Irifune, K. Terashima, H. Takeya, Y. Nakamoto, K. Shimizu, and Y. Takano, Supercond. Sci. Technol. **33**, 124005 (2020).
[9] D. V. Semenok, A. G. Kvashnin, A. G. Ivanova, V. Svitlyk, V. Y. Fominski, A. V. Sadakov, O. A. Sobolevskiy, V. M. Pudalov, I. A. Troyan, and A. R. Oganov, Materials Today **33**, 36 (2020).
[10] W. Chen, D. V. Semenok, X. Huang, H. Shu, X. Li, D. Duan, T. Cui, and A. R. Oganov, Phys. Rev. Lett. **127**, 117001 (2021).
[11] P. Kong, V. S. Minkov, M. A. Kuzovnikov, A. P. Drozdov, S. P. Besedin, S. Mozaffari, L. Balicas, F. F. Balakirev, V. B. Prakapenka, S. Chariton, D. A. Knyazev, E. Greenberg, and M. I. Eremets, Nat Commun **12**, 5075 (2021).
[12] I. A. Troyan, D. V. Semenok, A. G. Kvashnin, A. V. Sadakov, O. A. Sobolevskiy, V. M. Pudalov, A. G. Ivanova, V. B. Prakapenka, E. Greenberg, A. G. Gavriliuk, I. S. Lyubutin, V. V. Struzhkin, A. Bergara, I. Errea, R. Bianco, M. Calandra, F. Mauri, L. Monacelli, R. Akashi, and A. R. Oganov, Advanced Materials **33**, 2006832 (2021).
[13] Z. Li, X. He, C. Zhang, X. Wang, S. Zhang, Y. Jia, S. Feng, K. Lu, J. Zhao, J. Zhang, B. Min, Y. Long, R. Yu, L. Wang, M. Ye, Z. Zhang, V. Prakapenka, S. Chariton, P. A. Ginsberg, J. Bass, S. Yuan, H. Liu, and C. Jin, Nat Commun **13**, 2863 (2022).
[14] L. Ma, K. Wang, Y. Xie, X. Yang, Y. Wang, M. Zhou, H. Liu, X. Yu, Y. Zhao, H. Wang, G. Liu, and Y. Ma, Phys. Rev. Lett. **128**, 167001 (2022).
[15] Y. Song, J. Bi, Y. Nakamoto, K. Shimizu, H. Liu, B. Zou, G. Liu, H. Wang, and Y. Ma, Phys. Rev. Lett. **130**, 266001 (2023).
[16] S. Cross, J. Buhot, A. Brooks, W. Thomas, A. Kleppe, O. Lord, and S. Friedemann, Phys. Rev. B **109**, L020503 (2024).
[17] H. Sun, M. Huo, X. Hu, J. Li, Z. Liu, Y. Han, L. Tang, Z. Mao, P. Yang, B. Wang, J. Cheng, D.-X. Yao, G.-M. Zhang, and M. Wang, Nature **621**, 493 (2023).
[18] H. Sakakibara, M. Ochi, H. Nagata, Y. Ueki, H. Sakurai, R. Matsumoto, K. Terashima, K. Hirose, H. Ohta, M. Kato, Y. Takano, and K. Kuroki, Phys. Rev. B **109**, 144511 (2024).
[19] X. Liu, P. Jiang, Y. Wang, M. Li, N. Li, Q. Zhang, Y. Wang, Y.-L. Li, and W. Yang, Phys. Rev. B **105**, 224511 (2022).
[20] C. Zhang, X. He, C. Liu, Z. Li, K. Lu, S. Zhang, S. Feng, X. Wang, Y. Peng, Y. Long, R. Yu, L. Wang, V. Prakapenka, S. Chariton, Q. Li, H. Liu, C. Chen, and C. Jin, Nat Commun **13**, 5411 (2022).
[21] J. Ying, S. Liu, Q. Lu, X. Wen, Z. Gui, Y. Zhang, X. Wang, J. Sun, and X. Chen, Phys. Rev. Lett. **130**, 256002 (2023).
[22] W. Buckel and R. Hilsch, Z. Physik **138**, 109 (1954).
[23] B. Abeles, R. W. Cohen, and G. W. Cullen, Phys. Rev. Lett. **17**, 632 (1966).
[24] J. W. Garland, K. H. Bennemann, and F. M. Mueller, Phys. Rev. Lett. **21**, 1315 (1968).
[25] M. Strongin, O. F. Kammerer, J. E. Crow, R. D. Parks, D. H. Douglass, and M. A. Jensen, Phys. Rev. Lett. **21**, 1320 (1968).
[26] M. Tian, J. Wang, J. S. Kurtz, Y. Liu, M. H. W. Chan, T. S. Mayer, and T. E. Mallouk, Phys. Rev. B **71**, 104521 (2005).
[27] M. H. Beutel, N. G. Ebensperger, M. Thiemann, G. Untereiner, V. Fritz, M. Javaheri, J. Nägele, R. Rösslhuber, M. Dressel, and M. Scheffler, Supercond. Sci. Technol. **29**, 085011 (2016).
[28] W. Bang, T. D. Morrison, K. D. D. Rathnayaka, I. F. Lyuksyutov, D. G. Naugle, and W. Teizer, Thin Solid Films **676**, 138 (2019).
[29] D. P. Lozano, S. Couet, C. Petermann, G. Hamoir, J. K. Jochum, T. Picot, E. Menéndez, K. Houben, V. Joly, V. A. Antohe, M. Y. Hu, B. M. Leu, A. Alatas, A. H. Said, S. Roelants, B. Partoens, M. V. Milošević, F. M. Peeters, L. Piraux, J. Van de Vondel, A. Vantomme, K. Temst, and M. J. Van Bael, Phys. Rev. B **99**, 064512 (2019).
[30] K. Knorr and N. Barth, Solid State Communications **8**, 1085 (1970).
[31] K. Houben, S. Couet, M. Trekels, E. Menéndez, T. Peissker, J. W. Seo, M. Y. Hu, J. Y. Zhao, E. E. Alp, S. Roelants, B. Partoens, M. V. Milošević, F. M. Peeters, D. Bessas, S. A. Brown, A. Vantomme, K. Temst, and

M. J. Van Bael, Phys. Rev. B **95**, 155413 (2017).
[32] K. Houben, J. K. Jochum, S. Couet, E. Menéndez, T. Picot, M. Y. Hu, J. Y. Zhao, E. E. Alp, A. Vantomme, K. Temst, and M. J. Van Bael, Sci Rep **10**, 5729 (2020).
[33] J. D. Barnett, V. E. Bean, and H. T. Hall, Journal of Applied Physics **37**, 875 (2004).
[34] A. Salamat, R. Briggs, P. Bouvier, S. Petitgirard, A. Dewaele, M. E. Cutler, F. Corà, D. Daisenberger, G. Garbarino, and P. F. McMillan, Phys. Rev. B **88**, 104104 (2013).
[35] G. Deffrennes, P. Faure, F. Bottin, J.-M. Joubert, and B. Oudot, Journal of Alloys and Compounds **919**, 165675 (2022).
[36] J. Wittig, Z. Physik **195**, 228 (1966).
[37] R. Matsumoto, Y. Sasama, M. Fujioka, T. Irifune, M. Tanaka, T. Yamaguchi, H. Takeya, and Y. Takano, Review of Scientific Instruments **87**, 076103 (2016).
[38] R. Matsumoto, T. Irifune, M. Tanaka, H. Takeya, and Y. Takano, Jpn. J. Appl. Phys. **56**, 05FC01 (2017).
[39] R. Matsumoto, A. Yamashita, H. Hara, T. Irifune, S. Adachi, H. Takeya, and Y. Takano, Appl. Phys. Express **11**, 053101 (2018).
[40] H. K. Mao, P. M. Bell, J. W. Shaner, and D. J. Steinberg, Journal of Applied Physics **49**, 3276 (2008).
[41] Y. Akahama and H. Kawamura, Journal of Applied Physics **96**, 3748 (2004).
[42] Y. Takano, M. Nagao, I. Sakaguchi, M. Tachiki, T. Hatano, K. Kobayashi, H. Umezawa, and H. Kawarada, Applied Physics Letters **85**, 2851 (2004).
[43] S. Adachi, R. Matsumoto, S. Yamamoto, T. D. Yamamoto, K. Terashima, Y. Saito, M. Esparza Echevarria, P. Baptista de Castro, P. Song, S. Iwasaki, H. Takeya, and Y. Takano, Applied Physics Letters **116**, 223506 (2020).
[44] R. Matsumoto, S. Nakano, S. Yamamoto, and Y. Takano, Jpn. J. Appl. Phys. **60**, 090902 (2021).
[45] M. Mito, M. Hitaka, T. Kawae, K. Takeda, T. Kitai, and N. Toyoshima, Jpn. J. Appl. Phys. **40**, 6641 (2001).
[46] M. Mito, T. Imakyurei, H. Deguchi, K. Matsumoto, H. Hara, T. Ozaki, H. Takeya, and Y. Takano, J. Phys. Soc. Jpn. **83**, 023705 (2014).
[47] M. Mito, H. Goto, H. Matsui, H. Deguchi, K. Matsumoto, H. Hara, T. Ozaki, H. Takeya, and Y. Takano, J. Phys. Soc. Jpn. **85**, 024711 (2016).
[48] M. Mito, K. Ogata, H. Goto, K. Tsuruta, K. Nakamura, H. Deguchi, T. Horide, K. Matsumoto, T. Tajiri, H. Hara, T. Ozaki, H. Takeya, and Y. Takano, Phys. Rev. B **95**, 064503 (2017).
[49] M. Abdel-Hafiez, Y. Zhao, Z. Huang, C.-w. Cho, C. H. Wong, A. Hassen, M. Ohkuma, Y.-W. Fang, B.-J. Pan, Z.-A. Ren, A. Sadakov, A. Usoltsev, V. Pudalov, M. Mito, R. Lortz, C. Krellner, and W. Yang, Phys. Rev. B **97**, 134508 (2018).
[50] M. Mito, Y. Kitamura, T. Tajiri, K. Nakamura, R. Shiraishi, K. Ogata, H. Deguchi, T. Yamaguchi, N. Takeshita, T. Nishizaki, K. Edalati, and Z. Horita, Journal of Applied Physics **125**, 125901 (2019).
[51] T. Irifune, A. Kurio, S. Sakamoto, T. Inoue, and H. Sumiya, Nature **421**, 599 (2003).
[52] G. J. Dolan and J. Silcox, Phys. Rev. Lett. **30**, 603 (1973).
[53] M. Ohkuma, R. Matsumoto, and Y. Takano, Appl. Phys. Express **16**, 043004 (2023).
[54] E. Helfand and N. R. Werthamer, Phys. Rev. **147**, 288 (1966).
[55] N. R. Werthamer, E. Helfand, and P. C. Hohenberg, Phys. Rev. **147**, 295 (1966).
[56] T. Baumgartner, M. Eisterer, H. W. Weber, R. Flükiger, C. Scheuerlein, and L. Bottura, Supercond. Sci. Technol. **27**, 015005 (2013).
[57] Y. Zhang, C. H. Wong, J. Shen, S. T. Sze, B. Zhang, H. Zhang, Y. Dong, H. Xu, Z. Yan, Y. Li, X. Hu, and R. Lortz, Sci Rep **6**, 32963 (2016).
[58] Z. Shao, Z. Zhang, H. Yuan, H. Sun, Y. Cao, X. Zhang, S. Li, H. Gedeon, T. Xiang, Q.-K. Xue, and M. Pan, Science Bulletin **63**, 1332 (2018).
[59] R. E. Glover, Physics Letters A **25**, 542 (1967).
[60] L. G. Aslamasov and A. I. Larkin, Physics Letters A **26**, 238 (1968).
[61] W. J. Skocpol and M. Tinkham, Rep. Prog. Phys. **38**, 1049 (1975).
[62] D. Sóñora, C. Carballeira, J. J. Ponte, F. Vidal, T. Grenet, and J. Mosqueira, Phys. Rev. B **100**, 104509 (2019).
[63] S. Hsieh, P. Bhattacharyya, C. Zu, T. Mittiga, T. J. Smart, F. Machado, B. Kobrin, T. O. Höhn, N. Z. Rui, M. Kamrani, S. Chatterjee, S. Choi, M. Zaletel, V. V. Struzhkin, J. E. Moore, V. I. Levitas, R. Jeanloz, and N. Y. Yao, Science **366**, 1349 (2019).
[64] M. Lesik, T. Plisson, L. Toraille, J. Renaud, F. Occelli, M. Schmidt, O. Salord, A. Delobbe, T. Debuisschert, L. Rondin, P. Loubeyre, and J.-F. Roch, Science **366**, 1359 (2019).
[65] K. Umeo, Review of Scientific Instruments **87**, 063901 (2016).
[66] Z.-Y. Cao, H. Jang, S. Choi, J. Kim, S. Kim, J.-B. Zhang, A. S. Sharbirin, J. Kim, and T. Park, NPG Asia Mater **15**, 1 (2023).